JMEPEG (1994) 3:639-648

Simulation of Deep Penetration Welding of Stainless Steel Using Geometric Constraints Based on Experimental Information

S.G. Lambrakos, E.A. Metzbower, J. Milewski, G. Lewis, R. Dixon, and D. Korzekwa

Results of a numerical simulation of deep penetration welding of 304 stainless steel are presented. This numerical model calculates the temperature and fluid velocity fields in a three-dimensional workpiece undergoing deep-penetration electron beam welding. The deposition of power from the beam and energy outflow at the model-system boundaries is effected by means of time-dependent boundary conditions on the equations of energy and momentum transfer. The vapor-liquid interface defining the keyhole is represented by a surface whose temperature is that of vaporization for the steel. On this surface, are specified boundary conditions for the momentum transfer equations such that the component of the velocity normal to the keyhole vapor-liquid interface is zero. In addition, this study introduces two new numerical procedures. These procedures are based on the inclusion of experimental information concerning beam spot size and weld pool geometry into the model system via constraints and the deduction of effective keyhole shape via an inverse mapping scheme.

Keywords
deep penetration, geometric constraints, numerical modeling

1. Introduction

ANOTHER report (Ref 1) introduced a numerical model for calculating structures that can occur in deep penetration welding processes, i.e., laser or electron beam. That report describes the general features of this numerical model, i.e., the underlying physical model and the associated numerical methods. In addition Ref 1 gives a qualitative case study of the general influence of keyhole stirring on the melt pool and a general outline of those features of this model permitting its extension to relatively more quantitative analysis. This report describes the calculation of weld pool structures for deep penetration welding of 304 stainless steel. The physical approximations employed in this particular case study result from adopting the physical properties of 304 stainless steel as a function of temperature and from adjusting this model to include experimental information resulting from an analysis of specific cases of electron beam welding of 304 stainless steel. The Boussinesq approximation (Ref 2,3) is applied to the system of transport equations underlying this numerical model. This follows because a representation of the physical properties via a functional dependence on temperature implies certain specific assumptions regarding the timescale for local equilibration between fluid volume elements.

The modeling of deep penetration welding processes differs from the modeling of other welding processes in that the overall process consists of processes occurring at different temperatures within a range of temperatures between room temperature and the temperature of vaporization, T_G. In principle, this range of temperatures can even be extended above T_G if one includes processes occurring inside the keyhole where temperatures above T_G can occur. From the standpoint of numerical modeling, this implies that the problem has several aspects.

First, with respect to numerical methods for solving differential equations, the coupling between regimes defined by processes whose characteristic timescales are different means that the system is not only stiff but that stiffness can occur at different regions of the overall system.

Second, the physical character of the transport, both of energy and of momentum, is not the same for all the different regions making up the overall system. The upstream influence on structures increases with the degree of proximity to the keyhole.

Third, there are regions within the system at which either exothermic or endothermic reactions occur. These regions could be characterized by inherently unsteady or fine-scale structures. How to accurately represent the average influence of these structures in a steady-state sense poses an additional problem.

Reference 1 presents simulations for the purpose of a general qualitative analysis of structures occurring in deep penetration welding. This study represents a first stage toward effecting a quantitative analysis of deep penetration welding structures in a specific system, i.e., 304 stainless steel, for the eventual purpose of quantitative prediction of thermal histories of elements within the workpiece. In light of the goal of quantitative prediction, a model that combines processes occurring within the keyhole with diffusive and convective energy transfer in the liquid and solid, although feasible, is not optimal with respect to convenience or efficiency. This observation is completely natural because the characteristic timescales of structures in the neighborhood of the keyhole vapor-liquid boundary and of structures in the neighborhood of the liquid-solid boundary are sufficiently dissimilar to necessitate a partitioning of the problem. The dynamics of keyhole stability, development, and geometry are therefore a separate problem whose results can be

---

S.G. Lambrakos and **E.A. Metzbower,** Code 6324, Materials Science and Technology Division, Naval Research Laboratory, Washington, DC 20375-5000, USA; **J. Milewski, G. Lewis, R. Dixon,** and **D. Korzekwa,** MST-6, Los Alamos National Laboratory, Los Alamos, NM 87545 USA

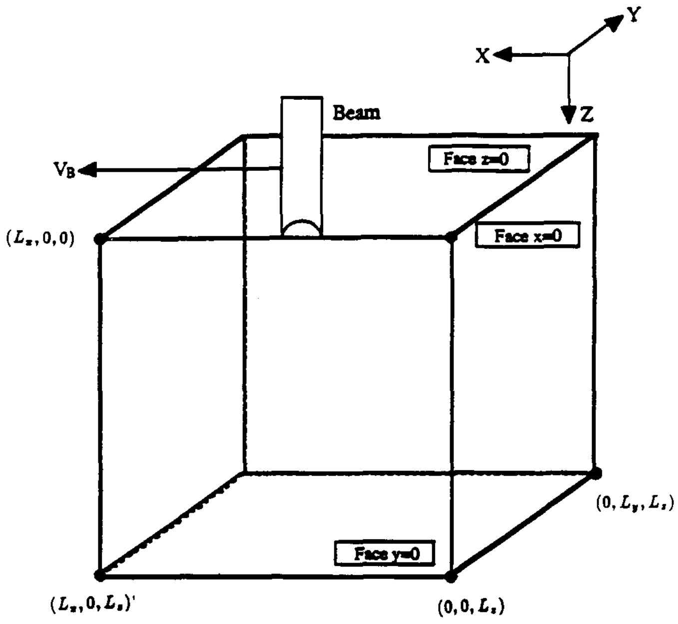

Fig. 1 Schematic of model system showing relative coordinates of system boundaries

input into a model of the liquid-solid domain as either boundary conditions or constraints on the system equations. Therefore this study also represents a first step toward a partitioning of the overall problem into separate problems that can be interfaced.

In addition to presenting a case study simulation of deep penetration welding of 304 stainless steel, this study introduces two new approaches, which are general and should contribute significantly to effecting a quantitative analysis of deep penetration welding structures. These approaches are based on the inclusion of experimental information concerning keyhole and weld pool geometry into the model system via constraints and the deduction of "effective" keyhole shape via an inverse mapping procedure. The procedure for imposing constraints has an added feature that it tends to compensate for either the unavailability of materials properties (see discussion in Ref 4) at temperatures close to the temperature of vaporization or gaps in knowledge concerning aspects of keyhole shape, or for that matter, general character. The inverse mapping procedure is similar to the direct-problem approach, which is first constructing a model based on one's knowledge and assumptions about the underlying physical processes, inputting into the model system the best available physical constants specifying the material properties, and finally, comparing the results of simulation and experiment. Our inverse-mapping approach adjusts portions of the keyhole surface according to physically consistent mappings of experimental information concerning the shape of the solidification boundary.

2. Physical Model of Deep-Penetration Welding of 304 Stainless Steel

The general features of this numerical model are an extension of those described in Ref 1. For the purpose of completeness in this development, however, some of those features are reviewed.

The model system to be specified is that of unsteady energy and momentum transport in a coordinate system that is fixed in the reference frame of a moving electron beam energy source. Figure 1 shows a schematic of the model system. The boundaries of the model system are defined, at each timestep, by the sides of a finite-sized rectangular segment, whose physical edges are far from the beam spot, and by the temperature of vaporization isotherm, which defines the boundary of the keyhole.

The system is assumed to be symmetric about the xz-face at $y = 0$ (see Fig. 1); thus, only one half the system is modeled. The equations governing the model system are:

$$\frac{\partial T}{\partial t} + \nabla \cdot [\mathrm{U}T] + \delta_{1j}V_B\frac{\partial T}{\partial x_j} = \kappa(T)\nabla^2 T(\mathrm{x}, t) + \nabla \cdot \mathrm{q} \qquad \text{(Eq 1)}$$

where

$$\kappa(T) = \frac{k(T)}{\rho(T)C_p(T)} \qquad \text{(Eq 2)}$$

and

$$\nabla \cdot \mathrm{q} = \nabla \cdot \mathrm{q}_b + \nabla \cdot \mathrm{q}_s + \nabla \cdot \mathrm{q}_l \qquad \text{(Eq 3)}$$

The term $\nabla \cdot \mathrm{q}_b$ represents energy transfer into the system resulting from the beam source. The term $\nabla \cdot \mathrm{q}_s$ represents energy released due to solidification, and $\nabla \cdot \mathrm{q}_l$ is energy absorbed at the onset of liquefaction.

$$\frac{\partial U_j}{\partial t} + \nabla \cdot (\mathrm{U}U_j) + \delta_{1j}V_B\frac{\partial U_j}{\partial x_j} = \nu(T)\nabla^2 U_j - \frac{1}{\rho(T)}\frac{\partial P}{\partial x_j} - \delta_{3j}\beta(T)g(T - T_M) \qquad \text{(Eq 4)}$$

where

$$\nu(T) = \frac{\mu(T)}{\rho(T)} \qquad \text{(Eq 5)}$$

$$\nabla \cdot \mathrm{U} = 0 \qquad \text{(Eq 6)}$$

where $j = 1, 2, 3$ denotes the Cartesian coordinates x, y, and z, respectively. The remaining quantities are defined as follows. The quantity $\mathrm{U} = (U_1, U_2, U_3) = (u, v, w)$ is the velocity field at a given point, and $\mathrm{x} = (x_1, x_2, x_3) = (x, y, z)$ is the Cartesian coordinate of that point. The quantity V_B is the speed of the beam moving in the direction of increasing x, and δ_{ij} is the Kronecker delta function. The quantity P is the pressure at a given point, and T is the temperature. The temperature-dependent density $\rho(T)$ is (Ref 5):

$$\rho(T) = (7984.0 - 0.2651T - 1.158 \times 10^{-4}T^2)[1 - u_s(T - T_M)] + (7551.0 - 0.1117T - 1.506 \times 10^{-4}T^2)u_s(T - T_M) \qquad \text{(Eq 7)}$$

The thermal expansivity $\beta(T)$ is:

$$\beta(T) = 2.168 \times 10^{-5} + 5.798 \times 10^{-10}T + 2.572 \times 10^{-12}T^2 \qquad \text{(Eq 8)}$$

The quantity $\mu(T)$ is the coefficient of viscosity as a function of temperature and is approximated by:

$$\mu(T) = \mu_s[1 - u_s(T - T_M)] + \mu_l \qquad \text{(Eq 9)}$$

where

$$\mu_l(T) = 10^{-3.5958}10^{-(2385.2/T)} \qquad \text{(Eq 10)}$$

μ_s is a very large number representing an infinite viscosity in a solid, and $u_s(T - T_M)$ is a unit step function such that:

$$u_s(T - T_M) = 0 \qquad \text{(Eq 11a)}$$

if $T \le T_M$. Otherwise,

$$u_s(T - T_M) = 1 \qquad \text{(Eq 11b)}$$

The units of μ_l are kg/(m-s). The conductivity $k(T)$ is:

$$k(T) = (8.116 + 0.01618T)[1 - u_s(T - T_M)] + (12.29 + 3.248 \times 10^{-3}T)u_s(T - T_M) \qquad \text{(Eq 12)}$$

The units of $k(T)$ are in W/(m · K). The heat capacity $C_p(T)$ is:

$$C_p(T) = (433.506 + 0.124477T)[1 - u_s(T - T_M)] + (734.022)u_s(T - T_M) \qquad \text{(Eq 13)}$$

The units of $C_p(T)$ are in J/(kg · K). The thermal coefficient of surface tension is:

$$\frac{\partial \gamma}{\partial T} = -A_n f_s(x, y) \qquad \text{(Eq 14)}$$

where A_n is a constant and $f_s(x, y)$ is a two-dimensional modulation function whose form is specified according to experimental information about melt pool shape. The quantity given by Eq 14, which is formally equivalent to the coefficient of surface tension, is for lumping the influence of phenomena in the vicinity of the keyhole and at the surface, which are not included explicity in this model. Further discussion concerning this quantity is given below. Note, however, that this function provides a means for including experimentally obtained information concerning the geometry of the melt pool.

The source term $\nabla \cdot \mathrm{q}_s$ is specified according to the integral condition:

$$\int_t^{t+\Delta t} \nabla \cdot \mathrm{q}_s dt = \rho(T)\Delta_{\mathrm{fus}}H\delta_s(T - T_M) \qquad \text{(Eq 15)}$$

where

$$\int_{T_M - \Delta T}^{T_M} \delta_s(T - T_M)dT = 1 \qquad \text{(Eq 16)}$$

The sink term $\nabla \cdot \mathrm{q}_l$ is specified according to the integral condition:

$$\int_t^{t+\Delta t} \nabla \cdot \mathrm{q}_l dt = -\rho(T)\Delta_{\mathrm{fus}}H\delta_l(T - T_M) \qquad \text{(Eq 17)}$$

where

$$\int_{T_M}^{T_M+\Delta T} \delta_l(T - T_M)dT = 1 \qquad \text{(Eq 18)}$$

For Eq 16 and 18, ΔT is defined by:

$$\Delta T = \frac{\Delta_{\mathrm{fus}}H}{C_p(T_M)} \qquad \text{(Eq 19)}$$

where the heat of fusion $\Delta_{\mathrm{fus}}H = 2.47 \times 10^5$ J/kg. In the present calculation, $\nabla \cdot \mathrm{q}_l$ is assigned a value of zero. This approximation is based on the assumption of rapid onset of liquefaction and subsequent vaporization as is the case for these calculations.

Energy transfer into the system resulting from the beam source is effected via two procedures, which are equivalent. One procedure is to effect a temperature change ΔT_g in the neighborhood of the keyhole boundary according to the integral condition:

$$\int_t^{t+\Delta t} \nabla \cdot \mathrm{q}_b dt = \rho(T)C_p\Delta T_g\delta_b(T - T_G) \qquad \text{(Eq 20)}$$

where

$$\int_{T_G}^{T_G - \Delta T_g} \delta_b(T - T_G)dT = 1 \qquad \text{(Eq 21)}$$

The other procedure is to move the keyhole boundary through the system at a specified rate. Note that this procedure is equivalent to that defined by Eq 20 and 21.

In Eq 1 and 3, the influence of convection is represented by two terms; i.e., a term containing U and one containing V_B. This representation follows because the flow field associated with the convection terms in both the energy and momentum transport equations, i.e., Eq 1 and 2, is defined with respect to an origin that is fixed in the workpiece. The component of the flow field parallel to the direction of the motion of the beam is therefore $\rho(u + V_B)$; however, the dependent variables of the momentum transfer equations, (u, v, w), are the velocities relative to an origin that is stationary with respect to the beam. The weighting coefficients for the discretization of Eq 2 as defined by the SIMPLE algorithm (Ref 6) are modified to take into account this representation. In addition, although the weighting coefficients that are defined by SIMPLE are adopted here, the numerical procedure employed is different and is structured for this problem in particular.

At the keyhole liquid-vapor interface, the boundary conditions on the momentum transfer equations are those of a no-slip boundary. That is, the component of the velocity, in the reference frame of the workpiece, normal to the interface is zero:

$$\mathrm{U} \cdot \hat{\mathrm{n}} + \mathrm{V_B} \cdot \hat{\mathrm{n}} = 0 \qquad \text{(Eq 22)}$$

where $\hat{\mathrm{n}}$ is the unit normal to the keyhole liquid-vapor boundary and $\mathrm{V_B}$ is the velocity of the beam with respect to the workpiece and is in the x-direction. Another boundary on the molten region is defined by the solid-liquid interface. The boundary condition on this boundary is specified in our model according to:

$$U_j = -\delta_{1j} V_B \qquad \text{(Eq 23)}$$

if $T < T_M$.

Note that according to this specification, the set of all nodes having temperature values less than T_M includes both boundary and exterior points of the melt pool.

The effects of surface tension, energy transfer through the system boundaries of the workpiece, and energy transfer from the beam source enter the model via boundary conditions on the energy and momentum transport equations. The numerical procedure for effecting energy transfer through the system boundaries of the workpiece is discussed in the next section. Note again that the system boundaries do not correspond to the physical edge of the workpiece. The influence of surface tension and energy deposition from the beam onto the keyhole liquid-vapor boundary is not considered explicitly in this calculation. Remember that in Ref 1, the keyhole vapor-liquid interface was a time-dependent quantity, which evolved to a steady state along with the rest of the system. In that scheme, energy deposition from the beam is coupled into the system via an exponential penetration, which is physically consistent with energy deposition from a laser beam source. This approach is not followed in this study. Instead, an approach that facilitates the inclusion of experimental information concerning beam power and geometry is adopted. In addition, in Ref 1 calculations, the top boundary of the model system is considered to correspond to the physical edge of the workpiece. As a result, the coefficient of surface tension adopted in that calculation is meant to represent an approximation of that for a prototype iron-steel system. In this study, the top boundary of the system, in the liquid state, does not correspond to the physical top surface of the workpiece. Therefore, the coefficient of surface tension adopted in this calculation, although formally equivalent to a coefficient of surface tension, serves as a geometric-constraint parameter whose physical significance is that it facilitates the explicit inclusion of experimental information.

3. Boundary Conditions on Faces of Model System

This section specifies the boundary conditions on each face of the sample (see Fig. 1) with respect to temperature and velocity.

Boundary conditions on the xy-face at $z = 0$ are:

$$\frac{\partial T}{\partial z} = 0 \qquad \text{(Eq 24a)}$$

$$\mu \frac{\partial u}{\partial z} = -\frac{\partial \gamma}{\partial T} \frac{\partial T}{\partial x}$$

and

$$\mu \frac{\partial v}{\partial z} = -\frac{\partial \gamma}{\partial T} \frac{\partial T}{\partial y}$$

if

$$T_M \le T \le T_G \qquad \text{(Eq 24b)}$$

$$u = -V_B$$

and

$$v = 0 \qquad \text{(Eq 24c)}$$

otherwise, and:

$$w = 0 \qquad \text{(Eq 24d)}$$

The quantity $\partial \gamma / \partial T$ is the thermal coefficient of surface tension.

Boundary conditions on the xy-face at $z = L_z$ and at time $t + \Delta t$ are:

$$T(x, y, L_z, t + \Delta t) = \max\left[T_A, \frac{T(x, y, L_z - \Delta l, t)^2}{T(x, y, L_z - 2\Delta l, t)}\right] \qquad \text{(Eq 25a)}$$

$$\mu \frac{\partial u}{\partial z} = -\frac{\partial \gamma}{\partial T} \frac{\partial T}{\partial x}$$

and

$$\mu\frac{\partial v}{\partial z} = -\frac{\partial \gamma}{\partial T}\frac{\partial T}{\partial y} \tag{Eq 25b}$$

if

$$T_M \le T \le T_G$$

$$u = -V_B$$

and

$$v = 0 \tag{Eq 25c}$$

otherwise, and

$$w = 0 \tag{Eq 25d}$$

Boundary conditions on the xz-face at $y = 0$ are:

$$\frac{\partial T}{\partial y} = 0 \tag{Eq 26a}$$

$$\frac{\partial u}{\partial y} = 0,\ v = 0,\ \frac{\partial w}{\partial y} = 0 \tag{Eq 26b}$$

Boundary conditions on the xz-face at $y = L_y$ and at time $t + \Delta t$ are:

$$T(x, L_y, z, t + \Delta t) = \max\left[T_A, \frac{T(x, L_y - \Delta l, z, t)^2}{T(x, L_y - 2\Delta l, z, t)}\right]$$

$$u = -V_B,\ v = 0,\ w = 0$$

Boundary conditions on the yz-face at $x = 0$ and at time $t + \Delta t$ are:

$$T(0, y, z, t + \Delta t) = \max\left[T_A, \frac{T(\Delta l, y, z, t)^2}{T(2\Delta l, y, z, t)}\right] \tag{Eq 27a}$$

where $x = 0$ does not coincide with the physical edge of the workpiece.

$$u = -V_B,\ v = 0,\ w = 0 \tag{Eq 27b}$$

Boundary conditions on the yz-face at $x = L_x$ and at time $t + \Delta t$ are:

$$T(L_x, y, z, t + \Delta t) = \max\left[T_A, \frac{T(L_x - \Delta l, y, z, t)^2}{T(L_x - 2\Delta l, y, z, t)}\right] \tag{Eq 28a}$$

$$u = -V_B,\ v = 0,\ w = 0 \tag{Eq 28b}$$

Note that the boundary conditions on the system boundaries at face xz at $y = L_y$, face yz at $x = 0$, and face yz at $x = L_x$ are physically consistent since in these calculations a solid state occurs in the neighborhood of these boundaries. That is only if the temperature at grid points in the neighborhood of these boundaries is less than T_M so that $u = -V_B$.

4. Convenient Numerical Procedure for Calculating a Steady-State Solution via Successive Approximate Unsteady Solutions

Given a velocity field U_j^o, ($j = 1, 2, 3$) corresponding to time t and a pressure field P, then the velocity at time $t + \Delta t$ is:

$$U_{j,p} = \frac{1}{W_p}\left[\sum_{k=1}^{6} a_k U_{j,k} + \frac{\rho(\Delta l)^3}{\Delta t} U_{j,p}^o - \frac{\partial P_p}{\partial x_j} + B_j\right] \tag{Eq 29}$$

where

$$W_p = \sum_{k=1}^{6} a_k + \frac{\rho(\Delta l)^3}{\Delta t} \tag{Eq 30}$$

$j = 1, 2, 3$ and $(\Delta l)^3$ is the volume of each discrete volume element. In general, find P such that:

$$\sum_{j=1}^{3} \frac{\partial U_{j,p}}{\partial x_j} = 0 \tag{Eq 31}$$

Given that P^e is an estimate of the pressure, it follows that the corresponding velocity field $U_{j,p}^e$ calculated according to Eq 29 is such that:

$$\sum_{j=1}^{3} \frac{\partial U_{j,p}^e}{\partial x_j} \ne 0 \tag{Eq 32}$$

The problem is to determine the pressure field P^* which when added to P^e results in a velocity field that satisfies the continuity equation Eq 32. Adding a pressure field P^* to P^e is equivalent to adding a velocity field $U_{j,p}^c$ to $U_{j,p}^e$ given by:

$$U_{j,p}^c = -\frac{1}{W_p}\frac{\partial P_p^*}{\partial x_j} \tag{Eq 33}$$

such that:

$$\sum_{j=1}^{3}\left[\frac{\partial U_{j,p}^e}{\partial x_j} + \frac{\partial U_{j,p}^c}{\partial x_j}\right] = 0 \tag{Eq 34}$$

At this point, a convenient (and intermediate) relaxation coefficient, α^*_R, is introduced. Accordingly, a pressure correction, P^c_p, is defined such that:

$$P^c_p = \left(\frac{\alpha^*_R}{W_p}\right) P^*_p \qquad \text{(Eq 35)}$$

and therefore:

$$U^c_{j,p} = -\frac{1}{\alpha^*_R}\frac{\partial P^c_p}{\partial x_j} \qquad \text{(Eq 36)}$$

and adding a pressure field P^c_p is equivalent to adding a velocity field $U^c_{j,p}$ to $U^e_{j,p}$. Given P^e, a derivation of an expression for P^c is as follows. Substituting $U^c_{j,p}$ given by Eq 36 into 34:

$$\sum_{j=1}^{3} \frac{\partial U^e_{j,p}}{\partial x_j} - \frac{1}{\alpha^*_R}\sum_{j=1}^{3} \frac{\partial^2 P^c_p}{\partial x_j^2} = 0 \qquad \text{(Eq 37)}$$

Next note that if $\Delta x_j = \Delta l$ for $j = 1, 2, 3$, then:

$$\sum_{j=1}^{3} \frac{\partial^2 P^c_p}{\partial x_j^2} = \lim_{\Delta l \to 0} \frac{1}{\Delta l^2}\left[\sum_{k=1}^{6} P^c_k - 6P^c_p\right] \qquad \text{(Eq 38)}$$

In addition, a relaxation coefficient, α_R, is defined such that:

$$\alpha_R = \frac{(\Delta l)^2\, \alpha^*_R}{6} \qquad \text{(Eq 39)}$$

It follows from Eq 35, 38, and 39 that:

$$P^c_p \approx \frac{1}{6}\sum_{k=1}^{6} P^c_k - \alpha_R \sum_{j=1}^{3} \frac{\partial U^e_{j,p}}{\partial x_j} \qquad \text{(Eq 40)}$$

for the given set of coefficients a_k, which are iterated in time.

Our implementation of the above procedure for this calculation is defined by the following sequence of operations and is based relaxation via inertia, i.e., the timestep is used as a relaxation parameter. Let P^o_p be the pressure field corresponding to time t. One then calculates a velocity field U^e_p for the pressure field P^o_p and velocity field U^o_p according to Eq 29. Note the use of P^o_p for the estimated pressure field P^e_p defined above. Given the velocity field U^e_p, one then calculates the correction field P^c_p according to Eq 40. The pressure field corresponding to the current timestep is calculated according to:

$$P_p(t + \Delta t) = P^o_p + P^c_p \qquad \text{(Eq 41)}$$

5. Procedure for Imposing Constraints According to Experimental Information

In modeling the welding process at and in the vicinity of the keyhole, one is confronted with several problems. To begin with, the top surface of the melt pool is not flat, but rather extends above the top surface of the workpiece. An accurate representation of this structure is, in principle, very difficult. In order to accurately model the process that causes the expansion and flow of liquid out of the keyhole and onto the surface, one would have to know many details associated with the process occurring inside the keyhole. In addition, in order to model the flow of liquid along the nonflat beaded surface of the melt pool, one would have to know the geometry of the bead in the vicinity of the keyhole and the coefficient of surface tension for the entire range of temperatures between T_M and T_G. Further, there may be an unavailability of material properties, especially the coefficient of surface tension, for the full range of temperatures between T_M and T_G. And finally, the keyhole is typically comprised of inherently unsteady and sometimes turbulent structures.

With respect to the difficulty associated with accurately modeling the structures in the vicinity of the keyhole, the following proposition and basis for a new approach is presented. Namely, that the shape of the solidification boundary of the melt pool that intersects the top surface of the workpiece, which is underneath the material extending above the top surface, is the manifestation of all the processes occurring in the vicinity of and in the keyhole. Thus by adopting the shape of this two-dimensional structure as a geometric constraint, one is, in principle, accurately representing the combined influence of structures near and at the keyhole that are characterized by multiple differing characteristic length and time scales. The significant feature of this approach is that the exact shape of the solidification boundary at this plane is conveniently accessible experimentally. In the same spirit, the beam spot size and penetration depth represent additional structure information that may be input via geometric constraints.

The above approach is demonstrated by considering a case study involving an electron beam weldment produced by a beam of ~3 kW power and 3 cm/s welding speed. Cross sections for this weldment are shown in Fig. 2 and 3. In addition, the top surface view of a melted spot produced by turning the beam on for a short period of time is shown in Fig. 4. The geometric information obtained from an analysis of these cross sections and the observed beam spot size is used for the calculation shown in Fig. 5. For this calculation, the length of the keyhole is fixed to that of the measured penetration depth, and the radius of the keyhole is fixed to that of the measured spot size at the surface. A noticeable feature of the temperature contour corresponding to T_M is its ragged character. This is a discreteness effect due to the instantaneous release of energy due to solidification at a grid point whose temperature decreases below T_M; i.e., Eq 15 and 16. This effect can be smoothed out by adopting a finer grid and assuming implicitly some approximate rate for energy release. This issue, however, is not a subject of the present study.

The procedure for imposing the melt pool constraint at the top surface of the workpiece is effected by adjusting the values

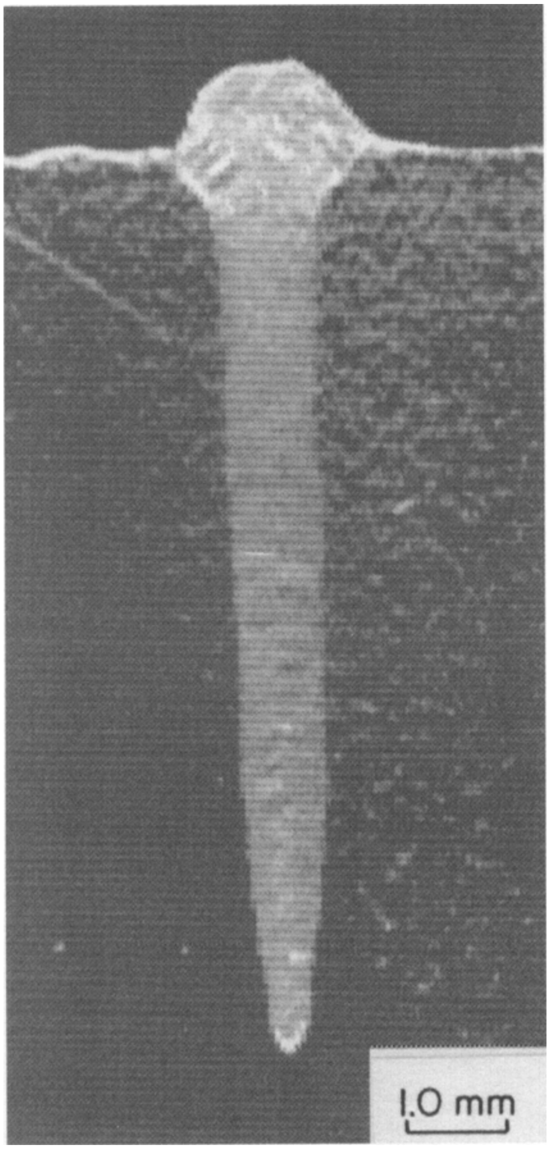

Fig. 2 Transverse cross section (i.e., *yz*-plane) of weld showing penetration depth and transverse extent of solidified melt pool. For this system, $V_B = 3$ cm/s, and the power into workpiece is ~3 kW. The depth of penetration is 7.75 mm (0.305 in.)

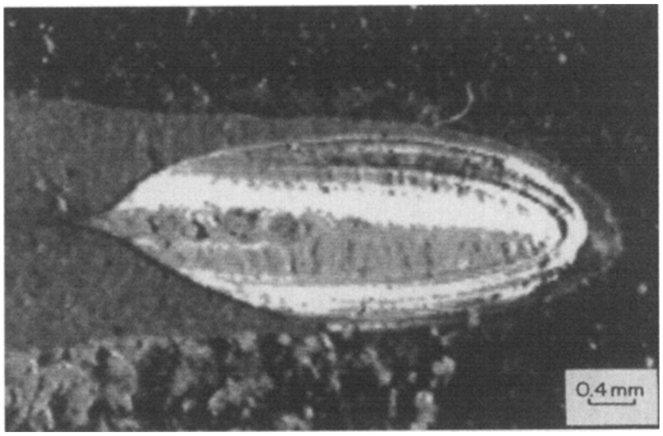

Fig. 3 Surface showing extent of melt pool on *xy*-plane corresponding to top surface of workpiece ($z = 0$), which is revealed by removing material extending above the surface. For this system, $V_B = 3$ cm/s, and the power into the workpiece is ~3 kW. The length and width, respectively, of this structure are 3.75 mm and 1.6 mm (0.148 in. and 0.063 in.)

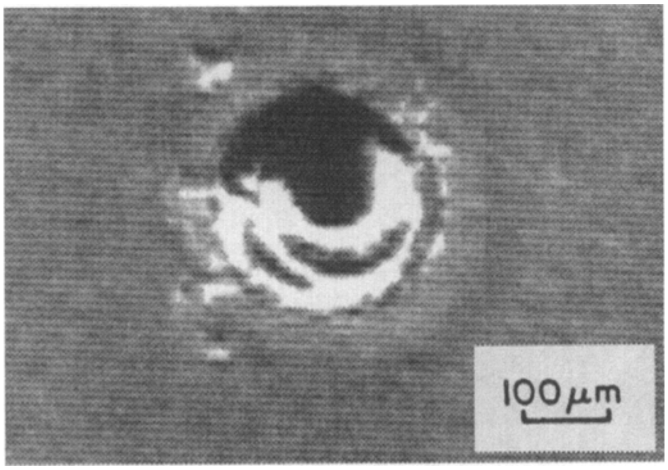

Fig. 4 Top surface view of a melted spot produced by turning beam on for ~0.25 s. The diameter of this spot is 0.232 mm (0.009 in.) and is made at sharp focus of the beam at the metal surface

of the surface-tension "like" coefficient defined by Eq 14. Note that although this coefficient has a formal similarity to that of a coefficient of surface tension, it no longer has this physical meaning. In addition, because the function of Eq 14 is for "weighting" the velocity field at the surface plane so as to effect the geometric constraint on the melt pool, the coefficient A_n may, in principle, be multiplied by a modulating function of x and y. For the calculation shown in Fig. 5(a), the value of A_n has been adjusted according to the measured length of melt pool feature shown at the surface plane along x (see Fig. 3). An adjustment with respect to the width of the melt pool, or for that matter its entire shape, is effected by multiplying A_n by an appropriate modulating (or shaping) function, i.e., $f_s(x, y)$ in Eq 14. For the calculation shown in Fig. 5(b), $f_s(x, y) = 1$ for all x and y. The calculation in Fig. 5 assumes that some type of estimate of the steady-state weld pool length can be obtained from experiment. Perhaps, however, this type of information is very difficult to obtain. It may be easier to obtain geometric information about the width, e.g., Fig. 2, and shape of the leading edge of the melt pool, e.g., Fig. 3. For the calculation shown in Fig. 6, the leading edge and width of the melt pool have been constrained approximately according to the observed width and shape of the melt pool shown in Fig. 2 and 3 using a modulating function $f_s(x, y)$.

The procedure for implementing constraints described in this section follows the direct problem approach. Further information concerning the shape of the keyhole below the top surface of the workpiece is input into the model system via the inverse mapping approach described in the next section.

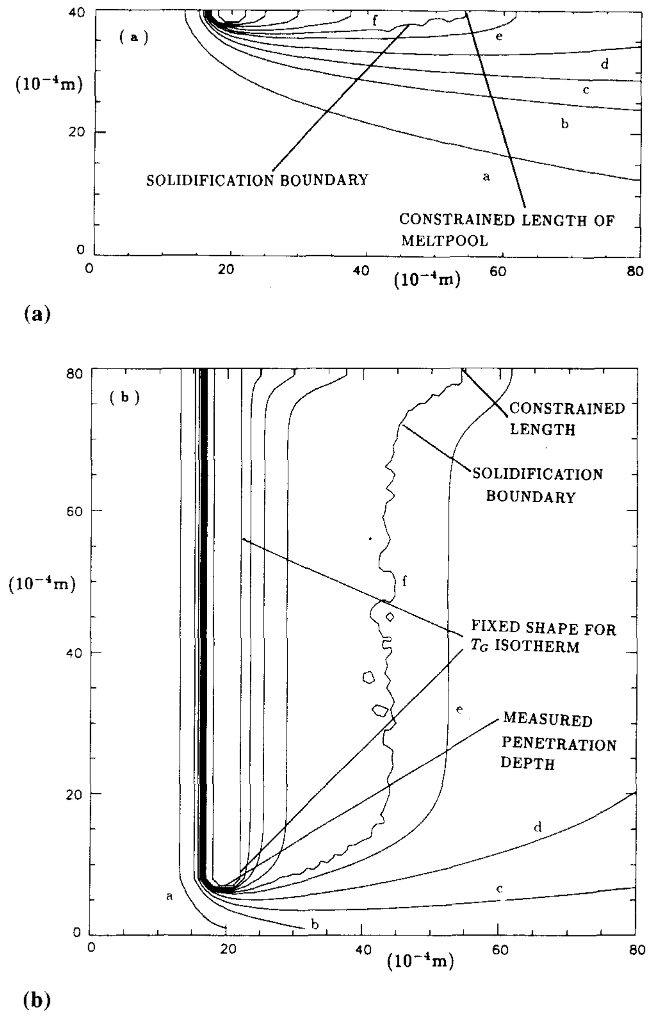

Fig. 5 Steady-state of model system for $V_B = 3$ cm/s and $A_n = 4 \times 10^{-6}$ where $n = 0$ (see Eq 14). The calculated power into the workpiece is ~1.5 kW. Shape of keyhole and melt pool partially constrained according to experimental information as that shown in Fig. 2, 3, and 4. The temperature isotherms are assigned as follows: a is 35 °C, b is 335 °C, c is 635 °C, d is 935 °C, e is 1235 °C, and f is T_M. In cases where isotherms are not labeled, temperatures are assigned as follows. The outermost isotherm is at 35 °C. Isotherms that are successively closer to the keyhole are at temperatures in the sequence 335 °C, 635 °C, 935 °C, 1235 °C, T_M, 1735 °C, 2035 °C, 2335 °C, and T_G

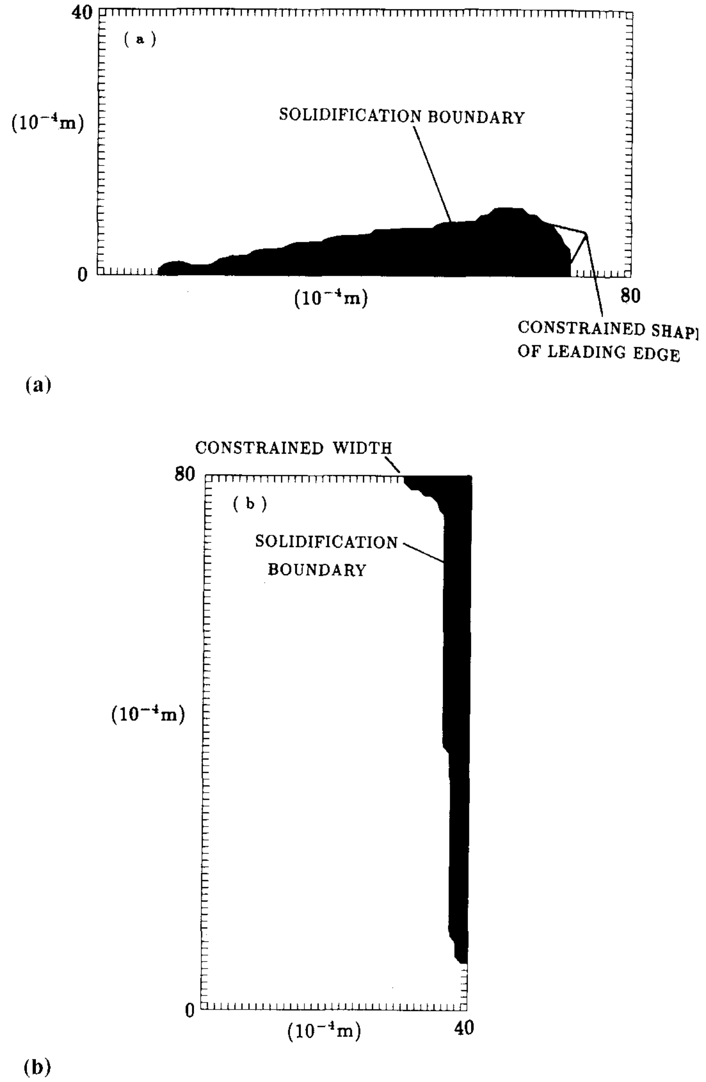

Fig. 6 Steady-state configuration of melt pool for model system where melt pool is partially constrained according to experimental information about width and steady-state shape of leading edge of melt pool. The parameter values are the same as for the calculation shown in Fig. 5

6. Inverse Mapping Procedure for Specifying Effective Shape of Keyhole

The procedure described in the above section uses the formalism of surface tension driven flow for imposing constraints associated with the melt pool geometry at the plane corresponding to the top surface of the workpiece. In that procedure, the geometry of the keyhole, i.e., the steady-state isotherm for the temperature of vaporization, is assumed given, and the surface tension coefficient is adopted as an adjustable parameter. This section describes a procedure for imposing constraints according to any available information concerning the shape of the melt pool below the surface of the workpiece. The shape of the keyhole below the surface is adopted as an adjustable parameter. In this procedure, the two-dimensional shape of the melt pool at the top surface of the workpiece is assumed given.

With respect to the difficulties discussed in the previous section associated with modeling accurately structures occurring in the vicinity of the keyhole, and in this case underneath the top surface of the workpiece, the following proposition and basis for another approach is presented. Namely that the three-dimensional surface of the solidification boundary of the melt pool below the surface of the workpiece is the manifestation of all the processes occurring in the vicinity of the keyhole as a time average given that the top surface geometry is constrained to the final fusion zone geometry. Further, all structures occurring inside the melt pool are only strongly coupled to the iso-

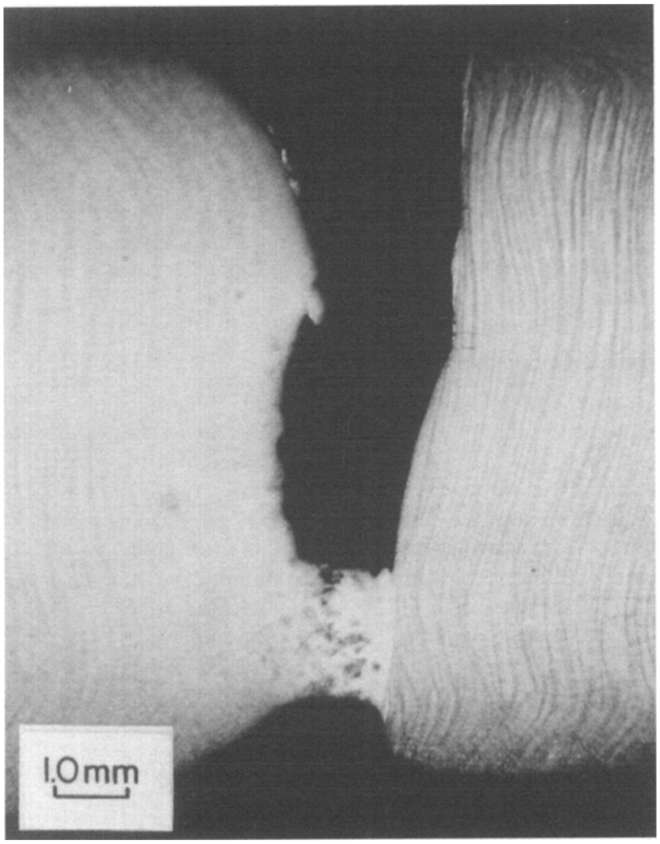

Fig. 7 A longitudinal slice of a weld parallel to the *zx*-plane, along the direction of motion of the beam relative to the workpiece, and passing approximately through the center of the beam. Solidification lines before and after welding are separated by a frozen keyhole. Solidification lines on the left of the keyhole tend to bend over while those on the right of the keyhole tend to be straight

thermal surface corresponding to the temperature of vaporization T_G. There is, therefore, a strong mapping between the shape of the keyhole and the shape of the melt pool below the surface given that the geometry of structures occurring on the surface is specified. In this approach, however, an inverse mapping procedure is followed. Information concerning the shape of the solidification boundary is assumed known, and the shape of the keyhole is adjusted to be consistent with this shape. An important aspect of this procedure is that information concerning the shape of the melt pool is more readily accessible than that of the keyhole.

We demonstrate the above approach by considering an adjustment, or refinement, of the keyhole surface according to information about the shape of the melt pool intersecting a longitudinal slice of the weld along the *xz*-plane passing through the center of the beam along the direction of motion of the beam relative to the workpiece. Shown in Fig. 7 is a frozen keyhole whose exact shape is not important for the present discussion. The direction of beam travel is from left to right. A comparison of solidification lines on the left to those on the right shows a bending of the solidification boundary on the left of the keyhole. Figure 8 shows that changes in the shape of the keyhole can be mapped onto the solidification boundary. For this calculation, the radius of the keyhole is reduced to half its value beyond a certain depth (4 mm, or 0.157 in.) within the workpiece. This keyhole shape results in a bending of the solidification boundary, which is qualitatively the same as that observed in Fig. 7.

7. Discussion

The authors extended a general numerical model previously developed and applied in a qualitative study (Ref 1) for its application to a quantitative analysis of deep penetration welding structures. The particular extension presented here is associated with a new approach, which uses experimental information concerning melt pool and keyhole geometry. Although the approach described here is for a quantitative analysis, the results of calculations presented are primarily for demonstrating the application of this approach. Several issues must be addressed before a quantitative analysis yielding an accurate thermal cycle function $T(t, x, y, z)$ is undertaken. These issues are the focus of the current study and are as follows.

The authors adopted the formalism of the surface tension coefficient for imposing geometry constraints associated with the shape of the melt pool at the top surface of the workpiece. In these calculations, the value of this quantity is adjusted only so that the length, width, or steady-state shape of the leading edge of the melt pool is consistent with experimental measurements. This, however, represents only partial information concerning the shape of the melt pool at the top surface. In order to adjust the calculated melt pool at the top surface so that it is consistent with experimentally observed structures, one must select the appropriate two-dimensional modulation function $f_s(x, y)$. Having done this, there still remains the issue of the sensitivity of the calculated melt pool boundary with respect to variations in the gradient of $f_s(x, y)$.

The inverse mapping procedure for specifying the effective shape of the keyhole encompasses several issues that must be addressed. First, given that one has deduced from experimental measurements sufficient information about the three-dimensional surface corresponding to the solidification boundary, one must effect a tractable and convenient procedure for adjusting the effective keyhole shape so that the calculated solidification boundary coincides with the experimentally deduced surface. Next, there is the issue of sensitivity of the calculated solidification boundary with respect to changes in the shape of the keyhole surface. Keep in mind that there is an inherent stiffness that develops with respect to the coupling between elements of the workpiece at positions progressively closer to the keyhole. This results from the substantial increase in magnitude of the temperature gradient for positions close to the keyhole. This stiffness can, in principle, introduce significant errors in the mapping between the effective keyhole surface and the solidification boundary.

There remains the issue of what can be considered appropriate geometric information. The solidification boundary consists of unsteady structures and does not achieve a fixed steady-state shape. However, experimental observation suggests that the solidification surface can be decomposed into two parts. One part, the smaller, is a time varying contribution. The

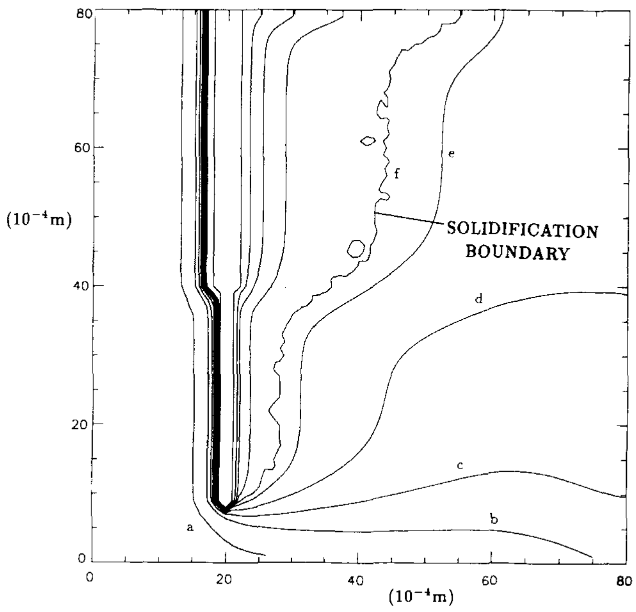

Fig. 8 Steady-state of model system with adjustment of keyhole geometry according to inverse mapping approach. That is to say, the shape of the effective keyhole surface is adjusted according to a specified shape of the liquid-solid boundary. The parameter values for this calculation are the same as those for the calculation shown in Fig. 5

larger part is a fixed surface, which maps onto a fixed keyhole surface corresponding to the time average of the variations in keyhole shape with respect to the timescale of thermal conduction in the liquid. An accurate specification of this steady-state component of the solidification boundary remains an open question for process development.

It is appropriate to state explicitly the goal underlying the development of this numerical model. Given a metallographic weld cross section in keyhole mode and that issues associated with numerical accuracy have been addressed, this model (via the inverse mapping approach) can, in principle, predict the temperature gradients around the weld pool as a function of time during the weld. These gradients must be known during solidification of the weld pool so that one may predict: elemental loss from the weld pool by vaporization; metallurgical structure of the weld; distortion from the weld process; and mechanical properties of the welded component at the weld based on metallurgical structure, mechanical properties, and stress state.

Acknowledgments

The authors would like to thank M. Remoissenet and the members of Laboratoire OSC at the Université de Bourgogne for the opportunity for further development of their welding model. This work was done while one author (S.G.L.) was Professuer invité at the OSC. Further, they would like to thank J.F. Paquerot for his discussions about numerical methods and his contributions toward further development of this model. And finally, the authors would like to thank K. Mahin for providing information concerning the bulk properties of 304 stainless steel.

References

1. S.G. Lambrakos, E.A. Metzbower, P.G. Moore, J.H. Dunn, and A. Monis, *J. Mater. Eng. Perform.*, Vol 2 (No. 6), 1993, p 819
2. R.K. Zeytounian, *Mécanique des fluides fondamentale*, Lecture Notes in Physics, Springer-Verlag, 1991, p 413
3. E.M. Sparrow, S.V. Patankar, and S. Ramadhyani, *Trans. ASME*, Vol 520 (No. 99), 1977
4. B.J. Keene, Review of data for surface tension of pure metals, *Inter. Mater. Rev.*, Vol 157 (No. 38), 1993, p 4
5. Coefficients and bulk properties as a function of temperature for 304 stainless steel, private communication with K. Mahin, Center for Materials and Applied Mechanics, Sandia National Laboratory
6. S.V. Patankar, *Numerical Heat Transfer and Fluid Flow*, Hemisphere Publishing, 1980